SPE-175018-MS

Society of Petroleum Engineers

Low Salinity Waterflooding in Carbonates Considering Mineralogy

Changhe Qiao, Li Li, Russell Johns, Jinchao Xu, the Pennsylvania State University

This paper was prepared for presentation at the SPE Annual Technical Conference and Exhibition held in Houston, Texas, USA, 28–30 September 2015.

Abstract

Modifying the injection brine composition has been shown to improve oil recovery (IOR) in carbonate reservoirs. Most of the existing numerical models for low salinity flooding are empirical and cannot capture important processes that involve aqueous species concentration, oil acidity and formation mineralogy. In our previous research (SPE170966), we developed a process-based model that explicitly includes the chemical interactions between crude oil, brine, and mineral surface. In this research, we extend the previous model to include mineral reactions and also extend the simulation from spontaneous imbibition to forced displacement.

In addition to the surface complexation and aqueous reactions presented in our previous model, calcite and anhydrite dissolution/precipitation are included to understand the role of mineralogy in low salinity flooding. The reaction laws are coupled with multiphase flow and transport. Relative permeability and residual oil saturation during flooding were dynamically adjusted according to the wettability. Those wettability-controlled functions were determined by the ratio of surface sites that contain the carboxylic group. An IMPEC method is used to numerically solve the coupled algebraic and differential equations. The model was tuned with core flooding experiments using various sets of carbonate rocks including Stevns Klint (SK) chalk, limestone (Austad et al. 2012), and middle east carbonate with anhydrite (Yousef et al. 2011).

The oil recovery curves were reproduced along with effluent concentrations of SO_4^{2-}, Ca^{2+} and Mg^{2+}. Simulation results demonstrate the recoveries for injection of various brines into carbonate rocks with and without anhydrite present. For limestone without anhydrite, increasing SO_4^{2-} concentration can lead to improved oil recovery (IOR) as much as 30% because of the increased SO_4^{2-} adsorption. For limestone with a small amount of anhydrite, the core is preferentially water wet initially and adding sulfate leads to anhydrite precipitation but the surface concentration of SO_4^{2-} remained unchanged. Injection of diluted formation water can significantly improve oil recovery (5% to 20% depending on the oil acidity) in the presence of anhydrite because the decrease of Ca^{2+} concentration enhances anhydrite dissolution and decreases the surface potential. The dissolution increased the sulfate concentration in the aqueous phase and on the rock surface, and the surface concentration of adsorbed carboxylic group decreased. This eventually leads to wettability alteration and improved oil recovery. When anhydrite does not exist, diluted formation water does not lead to IOR.

Introduction

Low salinity water (LSW) flooding was reported to effectively improve oil recovery (IOR) in sandstone and carbonate reservoirs (Yildiz and Morrow 1996; Lager et al. 2006; Yousef et al. 2010).

Substantial tietiary oil recovery was demonstrated at core scale through Amott imbibition test and coreflooding experiments with chalk and limestone cores (Zhang et al. 2007; Yousef et al. 2010; Fathi et al. 2010). The IOR effects were also confirmed at field scale, where diluted seawater was injected in a single well tracer test, and a reduction of residual oil saturation was confirmed (Yousef et al. 2012c).

Wettability alteration is a commonly accepted mechanism for LSW and was verified in several ways for carbonate rock material (Austad et al. 2008; Nasrella et al. 2014). The wettability of rock surface was altered from less water wet to more water wet when chemically tuned water is injected. The wettability alteration was demonstrated in chromatomatographic wettability test where more sulfate was adsorbed in water wet rock surface (Fathi et al. 2010). The wettability alteration was also shown in contact angle measurements on flat plane carbonate surface where smaller contact angle was reported for low salinity water (Alotaibi et al. 2010, Yousef et al. 2011). The wettability alteration reduced positive imbibition capillary pressure, as measured by sulfate free water and seawater that contains sulfate (Webb et al. 2005). Meanwhile, the shift of relative permeability and decrease of residual oil saturation was verified in experiments with varied pressure drop and flow velocity (Nasrella et al. 2014). The benefits of those wettability alteration was the improved oil recovery from 5% to 40% with spontaneous imbibition tests in Stevns Klint chalk and 5% to 20% with coreflooding experiments in middle east limestone (Fathi et al. 2010; Nasrella et al. 2014; Yousef et al. 2011).

There are a few proposed mechanisms for the observed wettability alteration. Mineral dissolution, surface adsorption/desorption and surface potential reduction were proposed as possible reasons that are responsible for the IOR (Hiorth et al. 2010; Tang and Morrow 1999; Zhang et al. 2007). Austad et al. (2008) identified that for Stevns Klint chalk outcrop, the concentration of potential determining ions (PDI) such as Mg^{2+}, Ca^{2+} and SO_4^{2-} and salinity greatly affected the oil recovery in spontaneous imbibition test. SO_4^{2-} gets adsorbed on the rock surface, alter the surface charge from positive to negative, and attracts positive cations Mg^{2+} and Ca^{2+} to solid surface to react with adsorbed carboxylic group. The release of carboxylic group from the chalk surface makes the surface more water wet. The carboxylic group release was also observed in Gomari et al. (2006) where the water vapor adsorption isotherm shows SO_4^{2-} reduced the adsorbed fatty acids surface concentration. The effects of PDIs are also demonstrated through changing the contact angle (Gupta et al. 2011) and imbibition capillary pressure (Webb et al. 2005). Besides SO_4^{2-}, BO_3^{2-} and PO_4^{3-} was also found to improve oil recovery (Gupta et al. 2011). The adsorption/desorption PDIs mechanism was moldeled using a reaction network representing the competitive adsorption/desorption reactions between oil, brine and rock in Qiao et al. (2014).

However experimental studies revealed that the effective brine formula is not necessarily effective for different other types of carbonates. Instead, diluted formation water and seawater was found to improve oil recovery for limestone and dolomites. As demonstrated in Yousef et al. (2010) and Nasrilla et al. (2014), improved oil recovery was observed repetitively using diluted formation water in core flooding experiments and altered wettability were verified contact angle measurements. Diluted formation water, even if without sulfate, was found to improve oil recovery by 5% (Strand et al. 2008). In some of the experiments that diluting formation water leads to IOR, anhydrite presence was reported (Austad et al. 2012; Yousef et al. 2011).

Those two conditions to achieve IOR for chalk and limestone were discussed in Romanuka et al. (2012), which conlude that the formulation of effective EOR fluids depends greatly on the rock mineralogy. As shown by a large scale screening Amott imbibition experiments, extra SO_4^{2-} does not lead to improved oil recovery for limestone and dolomite, while diluting the formation water does not lead to IOR for Stevns Klint chalk. One possible reason for sulfate free injection fluids IOR in limestone is the dissolution of anhydrite that insitu generate sulfate (Austad et al. 2012). Chandrasekhar et al. (2013) reported that extra SO_4^{2-} and Mg^{2+} can effectively improve oil recovery in core flooding experiments for limestone. However, the diluted sulfate free solution is also found effective for cores without anhydrite (Romanuka et al. 2012).

The wettability alteration in LSW was usually modeled by shifting the capillary pressure, relative permeability and residual oil saturation (Jerauld 2008; Al-Shalabi et al. 2014). The altered capillary pressure dorminates the improved oil recovery in spontaneous imbibition test (Yu et al. 2009; Qiao et al. 2014) while in core flooding experiments, the alteration of relative permeability curve and reduction of residual oil saturation dorminates the effect of coreflooding (Nasrella et al. 2014). The difference between mechanisitic model and empirical models lies in the difference in the weighing factor. In empirical models, the factors including the salinity, ionic strength, or total dissolved salts that are not direct indicator of wettability. In our mechanistic model, the concentration of surface species provide a direct wettability indicator. The advantage of a mechanistic model over an empirical model lies in that the mechanistic model is predictive on conditions that are not tested.

Using geochemical tools, the surface concentration is a function of the thermodynamic state (temperature), aqueous composition, oil and mineral properties. As the dominating mineral for carbonate rocks are calcite and the wettability alteration was caused by chemical reasons (Buckley et al. 1998), there should be a consistent and unique mechanism that covers the different cases for carbonate cores. In this paper, we extended the multiphase reactive transport model proposed in Qiao et al. (2014). An extended reaction network was developed to capture the competitive effects of chemical species activity and ionic strength. The extended reaction network was able to predict the wettability for chalk and limestone with a variety of injection water composition tested. This was the first mechanistic model that can predict both the effects of LSW in chalk and limestone.

This paper is organized as follows. In the methodology section, we first briefly introduce the multiphase reactive transport equations, and then describe the wettability alteration model and the extended multiphase reaction network. A workflow for simulation is given. In the results and discussion section, we present the numerical simulation results including the comparison of experimental data and simulation output, and the species chemical concentrations. The limitations and future improvements are also discussed.

Methodology

In this section, we introduce a complete set of equations to describe the coupled behaviors of the flow, transport and reactions. A reaction network is proposed to capture the relavant chemical reactions in aqueous phase, carbonate surface and oil surface. The equilibrium of the interacting system determines the surface species concentration. The multiphase fluid/rock functions were determined according to the oil-wet carboxylic group surface concentration. The model assumptions are as follows:

1. The pressure effect on the chemical reaction system can be neglected.
2. The cores and reservoirs are isothermal.
3. The oil and water is immiscible. The change in interfacial tension on the oil-water interface is neglectible since it is reported that reduction of oil water interfacial tension is not the mechanism of low salinity water flooding.
4. Surface complexations and aqueous reactions are at equilibrium at high temperature.
5. The anhydrite and calcite dissolution is either kineticly controlled or equilibrium controlled depdending on the calculated Damkholer number.
6. Ionic strength affects the activity of aqueous species and the extended Debye-Huckel model is applicable.
7. Surface potential of the oil and solid surface play an important role in the surface complexation. The Gramade equation is applicable to relate the surface charge, solution ionic strength and surface potential.
8. Oil components adsorption/desorption can be expressed by oil/water interface species and water/solid interface species interaction.
9. Carboxylic group desorption make the rock more water wet. Therefore, the surface concentration of carboxylic group can be used to indicate the wettability.

10. The wettability alteration changes the relative permeability, capillary pressure and residual oil saturation. For each oil/rock system, those wettability functions can are known at the extreme cases (most reachable water wettability and original oil/mixed wetability).
11. For core flooding, the effect of capillary pressure can be neglected.

According to the assumptions, the complete equation set is presented as follows.

Coupled Equation System. The fundamental physical laws in low salinity water flooding include the mass conservation of oil/water and chemical species, Darcy's law and chemical reaction equilibrium. We briefly introduce the general multiphase reactive transport equation system in this section and the specific reaction network will be discussed in next section.

Immiscible oil/water flow. The mass conservation equations of the immiscible oil and water fluid phases are as follows:

$$\frac{\partial}{\partial t}(\phi S_\alpha \rho_\alpha) + \nabla \cdot (\rho_\alpha \vec{u}_\alpha) = 0, \alpha = o, w. \tag{1}$$

Darcy's law governs the flow rate of different phases:

$$\vec{u}_\alpha = \frac{k k_{r\alpha}}{\mu_\alpha} \nabla (P_\alpha - \rho_\alpha g Z), , \alpha = o, w. \tag{2}$$

The pressure difference between oil and water phases is the capillary pressure:

$$P_{cow} = P_o - P_w. \tag{3}$$

The saturation relation completes the set of equations

$$S_o + S_w = 1. \tag{4}$$

The primary unknowns for the multiphase flow system are the pressure and water phase saturation.

Reactive Transport Model. For the chemical species reactive transport system, the mass conservation equation for the primary species p is as follows:

$$\frac{\partial}{\partial t}\left(M_p + \sum_{q=1}^{N_{sec}} \nu_{qp} M_q \right) + \nabla \cdot (F_p + \sum_{q=1}^{N_{sec}} \nu_{qp} F_q) = 0, \qquad p = 1, \dots, n_{pri}. \tag{5}$$

The surface species are assumbed to be immobile. The meaning of the symbols can be found in nomenclature and more details can be found in Qiao et al. (2014).

Wettability alteration. Empirical methods used proper interpolation of oil relative permeability and residual oil saturation to history match the pressure drop and oil recovery (Al-Shalabi et al. 2014). In this research we used a simple model as follows:

$$k^*_{rw} = (1-\theta)\, k^*_{rw,ww} + \theta k^*_{rw,ow}$$
$$k^*_{ro} = (1-\theta)\, k^*_{ro,ww} + \theta\, k^*_{ro,ow}$$

where $k^*_{ro,ww}$, $k^*_{rw,ww}$, $k^*_{ro,ww}$ and $k^*_{wo,ow}$ are the extreme cases for the most oil wet and most water wet state for the given oil/rock system. The Brooks-Corey formulation was used here to describe the relative permeability as a function of normalized fluid saturation (Anderson 1987). The relative permeability was assumed to depend on the normalized water saturation S^*:

$$k_{rw} = k^*_{rw} (S^*)^{n_w}$$

$$k_{ro} = k_{ro}^{*}(1 - S^{*})^{n_o}$$

where S^{*} was calculated as

$$S^{*} = \frac{S_w - S_{wi}}{1 - S_{wi} - S_{or}}.$$

Here S_{wi} is the initial water saturation. S_{or} is the residual oil saturation also depend on wettability:

$$S_{or} = (1 - \theta)S_{or}^{ww} + \theta S_{or}^{ow}.$$

The capillary pressure was assumed to be zero for the simulation of coreflooding experiments, as Nasrela et al. (2014) verified that LSW in core flooding is not due to the decreased capillary pressure, but due to a combined effect of relative permeability and reduced residual oil saturation. Examples of relative permeability curves in extreme cases are shown in **Fig.1**.

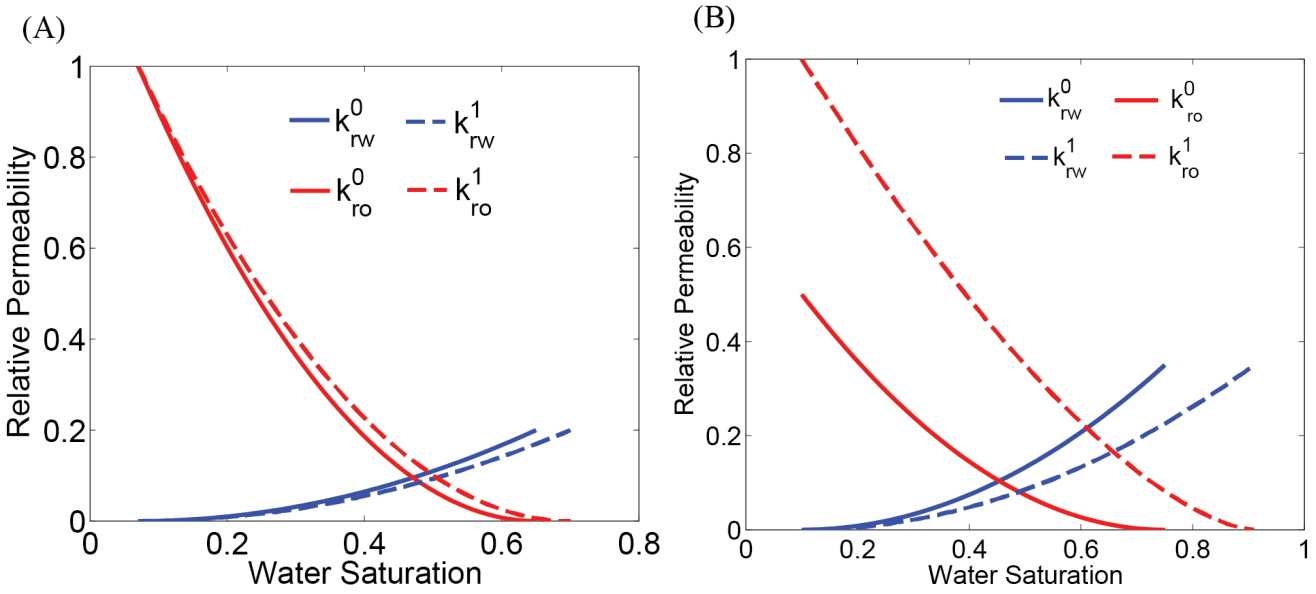

Figure 1 – Examples of relative permeability at the least and most water wet cases. k_{ro}^{0} and k_{rw}^{0} are relative permeability at the most oil wet wettability. k_{ro}^{1} and k_{rw}^{1} are the relative permeability at the most water wet wettability. (A) Relative permeability used in the simulation of the coreflooding experiments in Fathi et al. (2010). (B) Relative permeability used in the simulation of coreflooding experiments in Yousef et al. (2011).

Multiphase Reaction Network. The chemical reaction system includes chemical species and possible reactions, known as a reaction network. Here we extended the multiphase reaction network in Qiao et al. (2014) in order to represent more realistic conditions. We now include mineral dissolution/precipitation reactions, aqueous complexation and anionic surface site $> CO_3^-$. The extended reaction set is shown in **Table 1**. The primary species includes aqueous ions HCO_3^-, Cl^-, SO_4^{2-}, SCN^-, Mg^{2+}, Ca^{2+}, Na^+, K^+, H^+ and surface species $> CaOH_2^+$, $> CO_3^-$ and $-COO^-$, where ">" represent a solid surface species, and "–" represent a oil surface species. The reaction equilibrium constants are also listed. The reactions are discussed for each phase repectively as follows.

Aqueous phase. The species in aqueous phase can appear in free ion form and aqueous complex form. The considered species set includes free ions HCO_3^-, Cl^-, SO_4^{2-}, SCN^-, Mg^{2+}, Ca^{2+}, Na^+, K^+, H^+, CO_3^{2-}, OH^-, H_2CO_3 and aqueous complexations $MgSO_4$, $NaSO_4^-$, $CaSO_4$, $CaCl^+$, $MgCl^+$. The aqueous complexations greatly reduced the effective activity of PDIs (SO_4^{2-}, $Mg^{2+}$and Ca^{2+}) and reduced their

tendency to adsorb on the surface. The activity of the aqueous species was calculated from

$$a_i = \gamma_i C_i$$

where the activity coefficients were calculated according to the extended Debye-Hückel model (Helgeson et al. 1970, Qiao et al. 2014),

$$\ln \gamma_i = -\frac{Az_i^2\sqrt{I}}{1 + a_i^0 B\sqrt{I}} + bI.$$

The reaction equilibrium is modeled by a mass action law. For example, equilibrium for reaction (A4) is

$$K_{eq,A4} = \frac{a_{Mg^{2+}} a_{SO_4^{2-}}}{a_{MgSO_4}}.$$

where the activity of H_2O is unity. The reaction equilibrium coefficients for reactions (A1-A7) were from LLNL thermodynamic database ({Wolery, 1992 #28}).

The high Na^+ and Cl^- concentration reduces the PDIs' activity in two ways. First, the increased salt concentration increases the ionic strength, and the increased ionic strength reduces the activity coefficients of charged species. Second, the Na^+ and Cl^- can form ion pairs with PDIs in reactions (A5, A7, A8) and reduce the SO_4^{2-} concentration and activity.

Mineral reactions. There are two types of reactions on the mineral surface, mineral dissolution/precipitation and ion adsorption/desorption reactions. Both reactions depend on the mineral reactive surface area. For a specific mineral, the bulk reactive area is calculated as

$$[\text{Bulk surface area}] = [\text{moles}] \times [\text{molecular weight}] \times [\text{specific surface area}]$$

where moles of the mineral can be calculated from the volume fraction and molar volume as

$$[\text{mineral moles}] = \frac{[\text{mineral volume}]}{[\text{molar volume}]}.$$

The minerals considered relevant in this paper are calcite and anhydrite. Both minerals can dissolve or precipitate according to TST kinetic rate laws. One example of such reactions is

$$CaCO_3(s) + H^+ \leftrightarrow Ca^{2+} + HCO_3^-,$$

for which the reaction rate is written as

$$R_{CaCO_3(s)} = A_{CaCO_3(s)} k_{H^+} \exp\left(-\frac{E_a}{RT}\right) a_{H^+} \left(1 - \frac{a_{Ca^{2+}} a_{CO_2(aq)}}{K_{eq} a_{H^+}^2}\right).$$

A detailed description and explanation of the TST rate law can be found in Brantley et al. (2008). When the Damkholer number is greater than 10, the mineral reaction is assumed to be at equilibrium, namely

$$K_{eq} = \frac{a_{Ca^{2+}} a_{HCO_3^-}}{a_{H^+} a_{CaCO_3(s)}}.$$

where the activity of the mineral species is assumed to be unity. The reaction equilibrium constants were from LLNL thermodynamic database.

Solid surface complexation. Calcite surface contains surface sites that can adsorb aqueous ions and carboxylic groups. Calcite surface sites includes $>\mathrm{CaOH}$ and $>\mathrm{CO_3H}$. Other surface species $>\mathrm{CaOH_2^+}$, $>\mathrm{CaSO_4^-}$, $>\mathrm{CaCO_3^-}$, $>\mathrm{CO_3^-}$, $>\mathrm{CO_3Ca^+}$ and $>\mathrm{CO_3Mg^+}$ can also form. In this research two models can be used to describe the surface ractions, electrical diffusive layer (EDL) and non electrical diffusive layer (NEDL) model (Languir 1997). For the NEDL model, the equilibrium condition is as follows, taking reaction (C2) as an example,

$$K_{C2} = \frac{[> CaSO_4^-]}{[> CaOH_2^+]a_{SO_4^{2-}}}.$$

where $[> CaSO_4^-]$ and $[> CaOH_2^+]$ are the surface concentrations in units of mol/m^2. When an EDL model is be used, the activity of an aqueous species is corrected through a Boltzmann factor. For example, the equilibrium condition for reaction (C2) can be expressed as,

$$K_{C2} = \frac{\exp\left(-\frac{2F\psi_s}{RT}\right)[> CaSO_4^-]}{[> CaOH_2^+]a_{SO_4^{2-}}}.$$

The surface potential can be calculated from the Gouy-Chapman theory (Gouy 1910; Chapman 1913),

$$\sigma_s = -\sqrt{8\epsilon_0\epsilon_m IRT}\sinh\left(-\frac{F\psi_s}{2RT}\right).$$

where the notations can be found in Qiao et al. (2014). At 25°C, the surface potential degenerates to

$$\sigma_s = 0.1174\sqrt{I}\sinh(\frac{F\psi_s}{2RT}).$$

The reaction equilibrium constants were taken mainly from Parody et al. (1998) and Brady et al. (2012). A previous study uses the sensitivity analysis to demonstrate the strong dependency of the oil recovery on the reaction equilibrium constants (Qiao et al. 2014). The equilibrium contants depend on temperature and the correlation function between equilibrium constants and temperature is largely missing in the literature. For aqueous reactions, the $\mathrm{K_{eq}}$ values were intrinsic and well documented in a large range of temperature. For surface complexation, the $\mathrm{K_{eq}}$ values are empirical parameters that are related to intrinsic thermodynamic constants (Langmuir 1997). The $\mathrm{K_{eq}}$ values for each surface complexation can be determined for each specific rock surfaces. For example, the equilibrium constants for reactions (C1,C2) can be determined from matching the breakthrough curves.

Oil surface complexation. The active species are $-\mathrm{COOH}$, $-\mathrm{COO^-}$, $-\mathrm{COOCa^+}$ and $-\mathrm{COOMg^+}$. The $-\mathrm{NH_4}$ surface sites was excluded here as $-\mathrm{COO^-}$ dominates the association of oil and solid surface (Brady et al. 2010). The oil surface reactions are assumed to be only active at high temperature. The reaction equilibrium of oil surface reaction can be also modeled with either NEDL or EDL model in the same way as the solid surface reaction. The equilibrium condition and surface potential can be similarly calculated. Temperature effects for reactions on the oil surface were not significant according to Brady et al. (2012).

Interfacial interactions and wettability. The carbonate and water surfaces interaction was represented by the reaction (CO1) as proposed by Qiao et al. (2014). If the reaction goes from left to right, the system becomes more water wet as is in low salinity waterflooding. If the reaction goes from right to left, the system becomes more oil wet as happens in the aging procedure using crude oil. As this reaction is artificially created, the reaction equilibrium remained as a tunable factor according to different oil/rock system. The psudo-bonding species $[>\mathrm{CaOH_2^+}(-\mathrm{COO^-})]$ can therefore regarded as a relative wettability indicator of the surface. Therefore, the wettability factor θ is calculated from

$$\theta = \frac{c - c_{ww}}{c_{ow} - c_{ww}}$$

where c, c_{ww}, c_{ow} are the surface concentrations of $[> \mathrm{CaOH_2^+(-COO^-)}]$ at the current state, the most water wet state and the most oil wet state respectively. The surface concentration of $[> \mathrm{CaOH_2^+(-COO^-)}]$ for the extreme wettability cases are obtained by speciation calculation at the extreme conditions.

Simulation for different cases. Limestone and chalk have different properties, such as the porosity, permeability, pore structure, solid surface reactivity, and mineral composition. Those different properties lead to different response for chemically tuned brine injection. The chemical difference core samples were modeled to have different extrinsic properties such as specific surface area and total surface site density. The different parameters for limestone cores and outcrop chalk cores are listed in **Table 2**. A practical workflow for simulating coreflooding experiments is as follows.

1. Tune the k_{ro}, k_{rw} and S_{or} at the original wetting state so that the oil recovery is matched with formation water injected.
2. Find the k_{ro}, k_{rw} and S_{or} to match the ultimate recovery for the most water wet case. The relative permeability for the two extreme cases is used to predict the relative permeability at any intermediate state.
3. Perform the speciation calculation at the initial and injection condition. Select either the NEDL or EDL model so that the trend of wettability alteration is matched.
4. Perform simulation using the obtained extreme parameters.

Using this procedure, we simulated different coreflooding experiments in literature and the results are presented next.

Results and Discussion

In this section, we discuss the simulation results for a series of experiments using several carbonate rocks including the Stevns Klint (SK) Chalk (Fathi et al. 2010), a limestone (Strand et al. 2008), a limestone with anhydrite (Austad et al. 2012) and a Middle East limestone with anhydrite (Yousef et al. 2011). A one-dimensional model was used, where the porosity, permeability, oil/water viscosity, pressure and injection rate are given in **Table 3**. The water compositions reported in the corresponding literature were used as is in **Table 4**. This series of simulation is to demonstrate the capability of the model and establish a standard workflow to use this model.

Stevns Klint Chalk Outcrop. The wettability alteration in the SK chalk was shown by chromatographic wettability test. Both spontaneous imbibition tests and forced displacement experiments were performed. The oil recovery was demonstrated as a function of ionic composition, temperature and oil acidity. The chromatographic wettability tests and forced displacement simulation is demonstrated and compared with experimental results.

Chromatographic Wettability Test. A key mechanism of wettability alteration in the SK chalk was regarded to be due to the adsorption of SO_4^{2-} on the chalk surface (Austad et al. 2008). SO_4^{2-} adsorption can be quantified by the chromatographic wettability test, which provides a set of breakthrough curves for a nonreactive tracer and SO_4^{2-}. The SO_4^{2-} adsorption can be calculated by the area between the two breakthrough curves. The adsorped amount reflects the amount of surface sites available to adsorb SO_4^{2-}, which in turn can be used to quantify the surface area contacted by aqueous phase in the core.

Simulation were performed using all reactions except reactions (O1-O3), (CO1) and (M1-2). The oil surface reactions were excluded because at the core temperature the oil surface reaction were not regarded as active. Two coreflooding simulations were performed, with oil and without oil (Fathi et al. 2010). **Fig. 2A** shows the effluent curve in a completely water wet core in the absence of oil. **Fig.2B** shows the breakthrough curve with 0.53 water wet fraction in the presence of oil. The reduced adsorption in **Fig.2B** was achived by seting the specific surface area to be 0.53 m^2/g to mimic the fact

that some surface area are covered by oil. The diffusion/dispersion coefficient was determined by matching the tracer breakthrough curve. The effluent curves were matched using the reaction equilibrium constants for sulfate adsorption at room temperature. The simulated Mg^{2+} and Ca^{2+} breakthrough curves for both cases are shown in **Fig. 2C** and **2D**. As shown, Mg^{2+} replaces some of adsorbed Ca^{2+}.

Forced Displacement. In the forced displacement experiments (Fathi et al. 2010) at 120°C, FW,SW and SW0NaCl was successively injected with slug sized of 2 PV. The relative permeability was shown in **Fig. 1A**. The simulation reproduced the experiment oil recovery curve as demonstrated in **Fig. 3A**. The oil recovery demonstrate a sharp oil production and then the oil production was almost stopped, representing a water wet system. **Fig. 3B** shows the concentration of $[> CaOH_2^+(-COO^-)]$ at the last grid block, as is shown, stepwise reduction of the oil wettability is achieved. The predicted effluent curves of SO_4^{2-} and Ca^{2+} are given in Fig. 3B. A reduction of SO_4^{2-} concentration at the start of third stage was observed because of the increased adsorption in the core reduces SO_4^{2-} aqueous concentration.

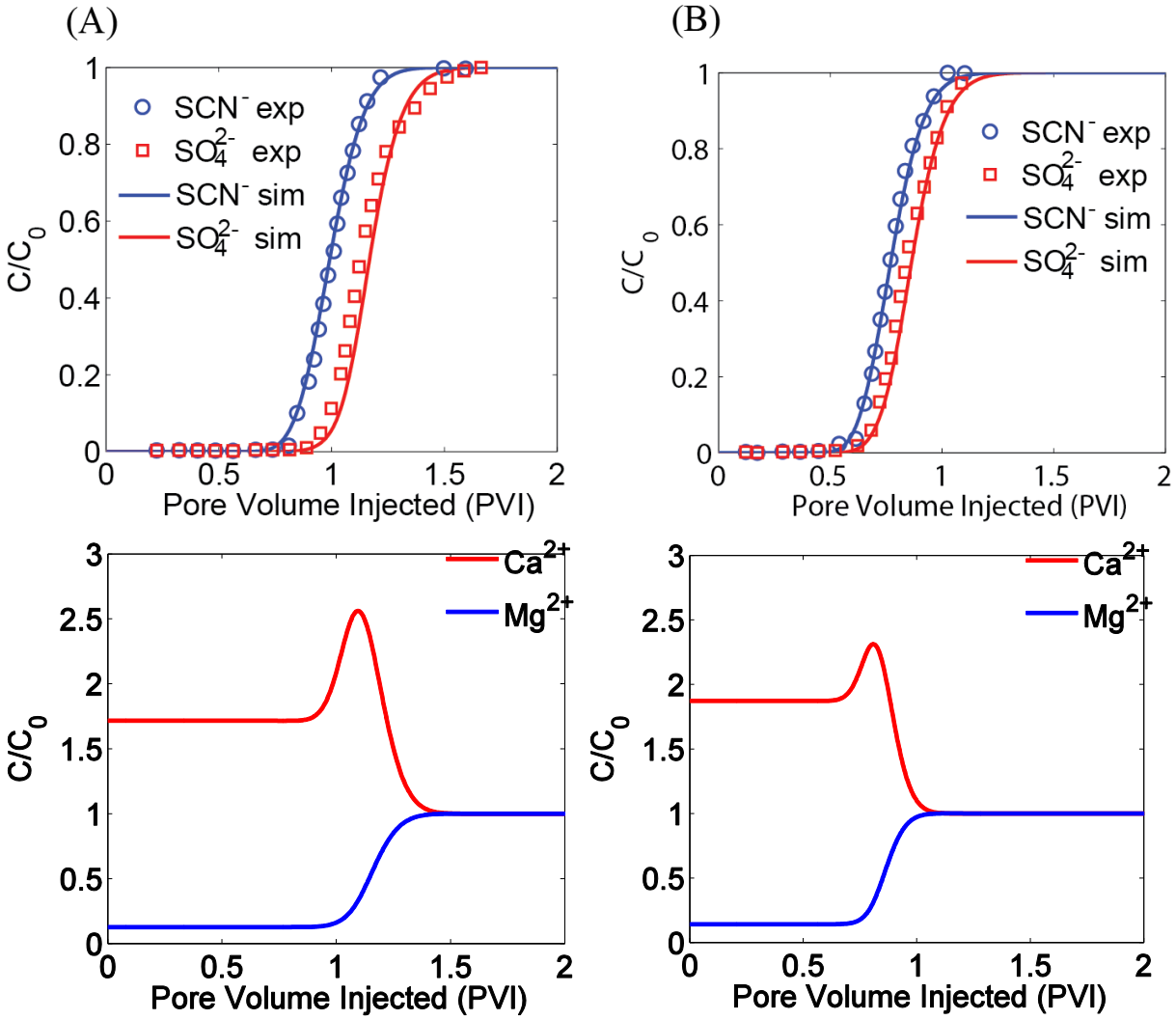

Figure 2: Effluent of seawater injection at room temperature. (A) Completely water wet. (B) Water wet fraction 0.53 in the presence of oil.

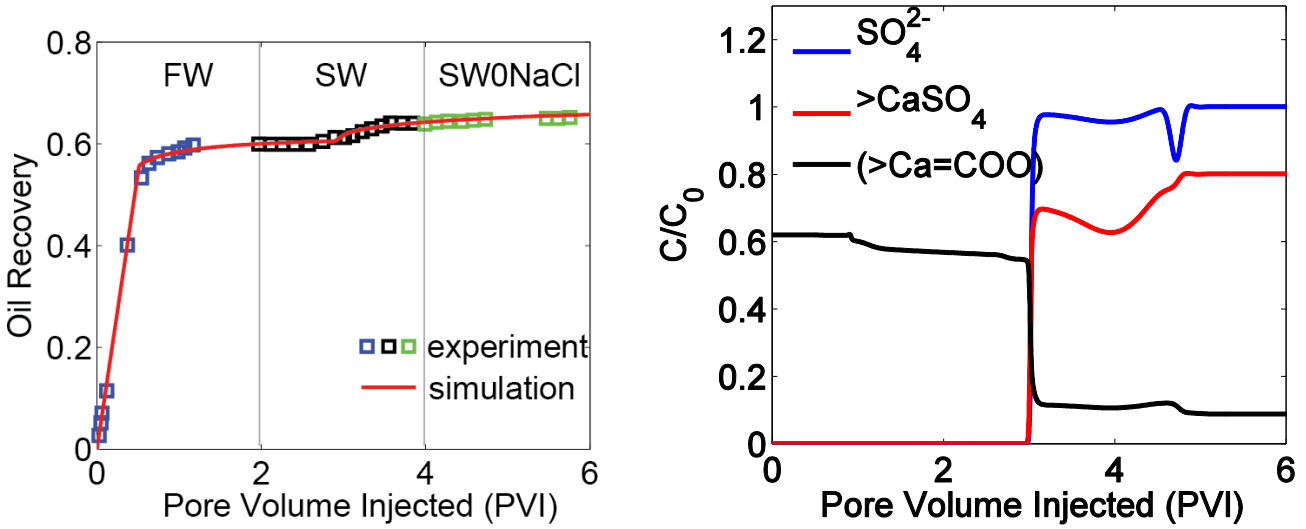

Figure 3 - Oil recovery for forced displacement. The experimental data is from Figure 11 in Fathi et al. (2010).

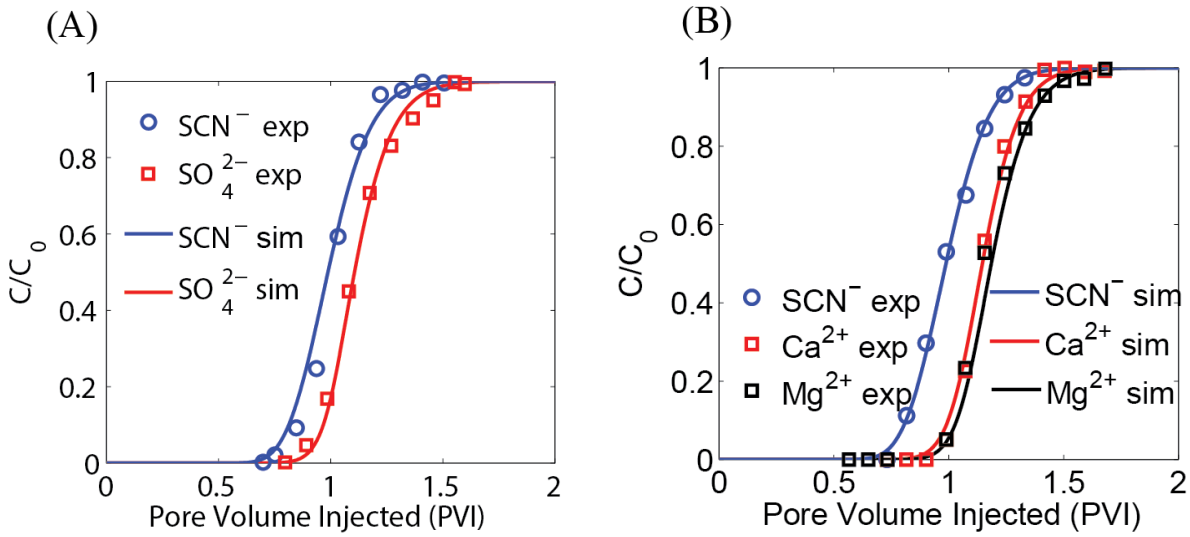

Figure 4: (A) Chromatographic wettability test with SCN^- and SO_4^{2-} in limestone cores at room temperature. The experimental data is from Strand et al. (2008). (B) SCN^-, Ca^{2+} and Mg^{2+} adsorption on limestone surface. The experimental data is from Strand et al. (2006).

Limestone Oil Reversoir Core. We next consider the simulation of experiments in limestone cores where brines with different compositions were injected and the effluent curves and oil recovery were compared with experiments. The purpose here is to examine the difference of reaction behavior of limestone compared to SC chalk and also to consider how the anhydrite dissolution reactions and how the dissolution affect the surface reactions. Similar with chalk, chromatographic wettability test and forced displacement experiments were performed and and compared to simulation data.

Chromatographic Wettability Test in Limestone. The purpose of this simulation is to explore the affinity of SO_4^{2-} towards to limestone surface. A chromatographic wettability test (Strand et al. 2008) at a complete water wet state was simulated and the effluent curves were matched. In the test, SW1/2M was injected into the limestone core and the composition can be found in Table 4. The differences than previous simulation was a smaller specific surface area (0.29 m^2/g) according to Sharipati et al. (2010) and a smaller diffusion/dispersion coefficient (0.002 ft^2/day) obtained by matching the tracer breakthrough curve. All other parameters remain the same and the details are shown in Table 3. As

shown in Fig. 4A, the simulation data agrees with the experimental data, which shows that the sulfate adsorption reaction is controlled by the same equilibrium condition.

Surface adsorption test for Ca^{2+} and Mg^{2+}. A solution (NaCl-M shown in Table 4) was injected to test the surface adsorption of Ca^{2+} and Mg^{2+} (Strand et al. 2008). Shown in **Fig. 4B**, Ca^{2+} and Mg^{2+} also adsorb on the surface in the absence of sulfate and oil. The experiment shows that the cat ion adsorption is independent from sulfate and oil, which can be described by the independent reactions (C4-C6). **Fig.5** shows the comparison of experimental and simulation effluent curves for SCN^-, Ca^{2+} and Mg^{2+} at 70°C. The effluent curves were matched with a slightly tuned K_{C4} and K_{C6} (-2.5 for both reactions) using the NEDL model.

The two simulations of chromatographic wettability tests show that there is no significant difference between chalk and limestone regarding the surface reactivity behaviors of Ca^{2+}, Mg^{2+} and SO_4^{2-}. In other words, the same reaction network can be used to describe the surface complexations on chalk and limestones.

Forced Displacement in Aqueous Zone Limestone Core with Anhydrite. Austad et al. (2012) observed tertiary improved oil recovery in limestone rocks with diluted sulfate free formation water. The presence of anhydrite was verified by flooding the core with distilled water. The forced displacement with core 5B in Austad et al. (2012) was simulated. As the injection rate is small (0.01 mL/min), the Damkholer number of calcite and anhydrite dissolution is large, i.e. 100 and 50 respectively. The mineral dissolution / precipitation is assumped to be at equilibrium.

Since the core material was sampled from the aqueous zone of a limestone reservoir, it is preferentially water wet even after aging, as the residual oil saturation was reached after breakthrough with formation water, as shown in the experimental data in **Fig.6**. Predicted oil recovery matched with the experimental recovery, while in both experimental data and simulation data the increase oil recovery was observed after approximately 1.1 PV of low salinity water injection.

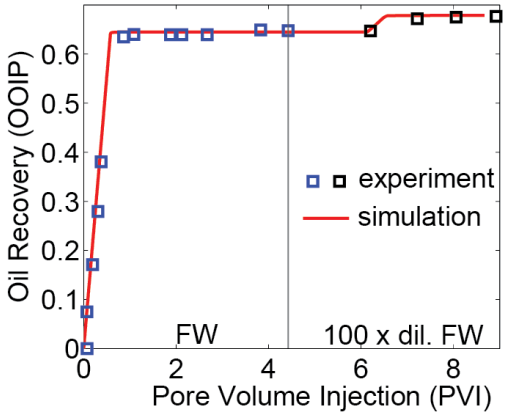

Figure 6 – Oil recovery for forced displacement in Austad et al. (2012).

Forced Displacement in Composite Limestone with Anhydrite. Yousef et al. (2011) reported that IOR was obtained with successive flooding composite carbonate cores with 2x, 10x and 20x diluted seawater. Meanwhile, the anhydrite presence was reported and dissolution was verified from NMR tests. The core was originally oil wet, as there is continuous oil production after water breakthrough. The surface concentration of water wet and oil wet cases were obtained from the model. An EDL model was used since the salinity was reported to greatly change the surface potential (Yousef et al. 2011). **Fig. 6** shows the oil recovery data from experiments and simulation. The match of the intermediate case shows the prediction capability of the model.

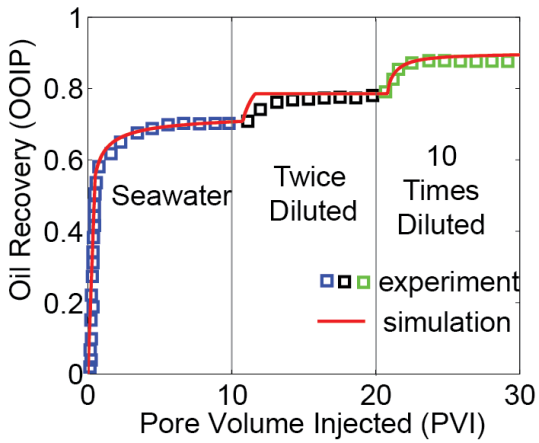

Figure 6 – Oil recovery for forced displacement in Yousef et al. (2010).

Model Limitations and Improvement. The complexity of the model is both the advantage and disadvantage. The model is an integrated system of many components, such as wettability alteration, multiphase flow and geochemistry. The solid surface adsorption of SO_4^{2-}, Ca^{2+}, and Mg^{2+} were validated in the absence of wettability alteration. The oil surface complexations were from the series work of Brady et al. The interfaction of oil surface and solid surface was hardly quantified in experiments. There lacks a step by step validation of such model with experiments under ideal conditions

Whether or not the EDL model could be used to predict the surface potential under the competitive adsorption is not validated. Moreover, an electrical double layer model could only be used after the experimentally measured surface potential was matched. A correlation of flat plane contact angle could be predicted and matched with experiments at different aqueous compositions. A triple layer model is probably needed so that the strongly bonded species and weakly bonded species could be distinguished. It was not validated what ions would be at the 0, β and d planes. The next fundamental step of this modeling research is to predict the zeta potential as measured in Alotaibi et al. (2011) and Nasrela et al. (2015).

Moreover, in the presence of Mg^{2+} and Ca^{2+} in limestone, dolomization reactions in limestone should be considered. Dolomite cores should also be considered.

Conclusions and Future Research

This model uses the surface competitive adsorptions involving SO_4^{2-}, Mg^{2+}, Ca^{2+} and carboxylic acid to explain the different cases of low salinity IOR (seawater in Stevns Klint chalk, diluted formation water and seawater in limestone containing anhydrite). The prediction of the effects of ionic composition, salinity, oil acidity and mineralogy were consistent with experimental data reported in the literature.

The mechanistic model plays an important role in understanding the mechanisms of the low salinity waterflooding. The developed model was used to predict the role of rock composition in determining IOR induced by wettability alteration for low salinity waterflooding for carbonates. The simulation results of spontaneous imbibition and forced displacement demonstrated that our model can capture the complex interactions among different phases, species and minerals. The model captures the role of mineral reactions in buffering the aqueous composition and was able to predict the wettability alteration owing to surface reactions. The oil recovery curves predicted for different brine compositions and minerals agree well with experimental data. This is the first mechanistic model for carbonate that considers rock composition and the coupling of mineral dissolution and surface complexation reactions. The simulation results also indicate that mineral dissolution can significantly affect the wettability alteration though buffering the aqueous concentration.

Nomenclature

ϕ is porosity (dimensionless); S, ρ, and $\vec{u}$ are the saturation (dimensionless), fluid density (kg/m^3), and volumetric flow rates (m^3/s) for the oil and water phases. The subscript "w" is for the water phase, and the subscript "o" is for the oil phase.

k is absolute permeability (m^2); Z is the depth (m); μ, g, and P are the viscosity (cP), gravitational constant (m/s^2), and the pressure of the fluid phase (Pa), respectively.

A_s is the bulk surface area (m^2) of mineral species s and is calculated from the specific surface area (SSA) and the mineral mass; $k_{r,l}$ is the reaction rate constant of the l^{th} path (mol/m^2·s); E_a is the activation energy (J/mol); R is the universal gas constant (8.31 J/mol·K); T is the temperature (K); n_{li} is the dependent exponent of species i for path l; IAP_r is the ionic activity product; $K_{eq,r}$ is the equilibrium constant.

References

Alotaibi, M., Azmy, R. and Rasr-El-Din 2010. Wettability Challenges in Carbonate Reservoirs.

Austad, T., Madland, M. and al., e. 2008. Seawater in Chalk: An EOR and Compaction Fluid.

Austad, T., Shariatpanahi, S. F., Strand, S., Black, C. J. J. and Webb, K. J. 2012. Conditions for a Low-Salinity Enhanced Oil Recovery (EOR) Effect in Carbonate Oil Reservoirs. Energy & Fuels 26 (1): 569-575. http://dx.doi.org/10.1021/ef201435g

Brantley, S. L., Kubicki, J. D. and White, A. F. 2008. Kinetics of water-rock interaction. Springer.

Chandrasekhar, S. and Mohanty, K. K. 2013. Wettability Alteration with Brine Composition in High Temperature Carbonate Reservoirs.

Fathi, J., Austad, T. and Strand, S. 2010. "Smart Water" as a Wettability Modifier n Chalk: The Effect of Salinity and Ionic Composition

Gupta, R., Smith, G. G., Hu, L., Willingham, T., Lo Cascio, M., Shyeh, J. J. and Harris, C. R. 2011. Enhanced Waterflood for Carbonate Reservoirs - Impact of Injection Water Composition. Paper presented at the http://dx.doi.org/10.2118/142668-MS

Nasrella, R., Sergienko, E. and Brussee, N. 2014. Demonstrating the Potential of Low Salinity Waterflood to Improve Oil Recovery in Carbonate Reservoirs by Qualitative Coreflood.

Romanuka, J., Hofman, J., Ligthelm, D. J., Suijkerbuijk, B., Marcelis, F., Oedai, S., Brussee, N., van der Linde, H., Aksulu, H. and Austad, T. 2012. Low Salinity EOR in Carbonates. Paper presented at the http://dx.doi.org/10.2118/153869-MS

Strand, S., Austad, T. and Puntervold, T. 2008. "Smart Water" for Oil Recovery from Fractured Limestone: A Prelimlinary Study. Energy & fuels

Yousef, A., Al-Saleh, S. and Al-Kaabi, A. 2011. Laboratory Investigation of the Impact of Injection-Water Salinity and Ionic Content on Oil Recovery From Carbonate Reservoirs. SPE REE

Table 1: Multiphase reaction network. The reaction equilibrium constants are from Parody et al. (1998), Brady et al. (2012) and Qiao et al. (2014).

Number	Reactions	K_{eq}(25)	K_{eq}(110)
Oil-water interface reactions			
O1	$-COOH \leftrightarrow -COO^- + H^+$	-5.0	-5.0
O2	$-COOCa^+ \leftrightarrow -COO^- + Ca^{2+}$	-1.2	-1.2
O3	$-COOMg^+ \leftrightarrow -COO^- + Mg^{2+}$	-1.0	-1.3
Calcite surface			
C1	$> CaOH + H^+ \leftrightarrow > CaOH_2^+$	11.8	11.8
C2	$> CaOH_2^+ + SO_4^{2-} \leftrightarrow > CaSO_4^- + H_2O$	-2.1	-3.25
C3	$> CaOH_2^+ + CO_3^{2-} \leftrightarrow > CaCO_3^- + H_2O$	6	6

C4	$> CO_3H \leftrightarrow > CO_3^- + H^+$	-5.1	-5.1
C5	$> CO_3Ca^+ \leftrightarrow > CO_3^- + Ca^{2+}$	-2.5	-3.4
C6	$> CO_3Mg^+ \leftrightarrow > CO_3^- + Mg^{2+}$	-2.5	-3.4
Calcite-water / Oil-water interface interaction			
CO1	$> CaOH_2^+(-COO^-) \leftrightarrow > CaOH_2^+ + -COO^-$	-	-5.9
Aqueous phase reactions			
A1	$H_2O \leftrightarrow H^+ + OH^-$	13.9991	12.24
A2	$HCO_3^- \leftrightarrow H^+ + CO_3^{2-}$	10.3288	10.27
A3	$H_2CO_3 \leftrightarrow H^+ + HCO_3^-$	-6.3477	-6.433
A4	$MgSO_4 \leftrightarrow Mg^{2+} + SO_4^{2-}$	-2.37	-2.4642
A5	$NaSO_4^- \leftrightarrow Na^+ + SO_4^{2-}$	-0.7	-0.7752
A6	$CaSO_4 \leftrightarrow Ca^{2+} + SO_4^{2-}$	-2.3	2.61
A7	$CaCl^+ \leftrightarrow Ca^{2+} + Cl^-$	-0.700	-0.54
A8	$MgCl^+ \leftrightarrow Mg^{2+} + Cl^-$	-0.1503	-0.74
Mineral reactions			
M1	$CaCO_3(s) + H^+ \leftrightarrow Ca^{2+} + HCO_3^-$	1.854	0.5871
M2	$CaSO_4(s) \leftrightarrow Ca^{2+} + SO_4^{2-}$	-4.3608	-5.34

Table 2 – Parameters of limestone and chalk.

	Chalk	Limestone
Specific surface area	2 m^2/g	0.17 ~ 0.29 m^2/g
$>$ CaOH site total density	4.1 μmol/m^2	4.1 μmol/m^2
$> CO_3H$ site total density	4.1 μmol/m^2	4.1 μmol/m^2
Anhydrite	0%	6%

Table 3 – Simulation inputs.

Reference	Fathi et al. (2010), SCC#1	Strand et al. (2008), Core 2-21	Austad et al. (2011), Core 5B	Yousef et al. (2011) 1st core flooding
Mineralogy	SK Chalk	Limestone	Limestone	Limestone
Porosity	0.45	0.25	0.18	0.251
Permeability	1 mD	2.7 mD	1.2 mD	39.6 mD
Specific surface area	1 m^2/g	0.29 m^2/g	0.29 m^2/g	0.29 m^2/g
Real dimensions	L: 70 mm D: 38.1 mm	L: 49 mm D: 37.8 mm	L: 81 mm D: 38 mm	L: 40.6 mm D: 38 mm
Simulation dimensions	0.2296 ft $\times$ (0.1108 ft)^2	0.1608 ft $\times$ (0.1105 ft)^2	0.265748 ft $\times$ (0.1107 ft)^2	0.133202 ft $\times$(0.1107 ft)^2
Initial wettability	Preferentially water wet	Weakly water wet	Preferentially water wet	Oil wet
Back pressure	145.03 psi	101.5 psi	145.03 psi	1000 psi
Injection rate	0.2 ml/min	0.1 ml/min	0.01 ml/min	5 ml/min
Oil viscosity	1 cp	1 cp	1 cp	1 cp
-COOH total surface site density	6 μmol/m^2	6 μmol/m^2	6 μmol/m^2	6 μmol/m^2
Water viscosity	0.476 cp	0.476 cp	0.476 cp	0.476 cp
Surface complexation model	NEDL	NEDL	NEDL	EDL

c_{ww}	0	-	1.35 $\mu mol/m^2$	0.03 $\mu mol/m^2$
c_{ow}	2.1 $\mu mol/m^2$	-	1.67 $\mu mol/m^2$	0.172 $\mu mol/m^2$
Diffusion /dispersion coefficient	0.0042 ft^2/day	0.002 ft^2/day	0	0

Table 4: Synthetic brine compositions used in experiments and simulations.

	FW[1]	SW[1]	SW0NaCl[1]	SW1/2M[2]	NaCl-M[2]	SW0NaCl4Ca
HCO_3^-	0.009	0.002	0.002	0.002	0.002	0.002
Cl^-	1.07	0.525	0.126	0.574	0.126	0.126
SO_4^{2-}	0	0.024	0.024	0.012	0.096	0.024
SCN^-	0	0	0	0.012		
Mg^{2+}	0.0008	0.045	0.045	0.045	0.045	0.045
Ca^{2+}	0.029	0.013	0.013	0.013	0.013	0.052
Na^+	1.00	0.450	0.050	0.475	0.050	0.050
K^+	0.005	0.01	0.01	0.022		
pH	8.4	8.4	8.4	8.4	8.4	8.4
Total Ionic Strength	2.198	1.305	0.506	0.410	0.794	0.662